R. & M. No. 3465

MINISTRY OF TECHNOLOGY

AERONAUTICAL RESEARCH COUNCIL
REPORTS AND MEMORANDA

The Pressure-Drag due to Blunt Leading Edges on Two-Dimensional Aerofoils, at Transonic and Low-Supersonic Speeds

by W. J. GRAHAM

LONDON: HER MAJESTY'S STATIONERY OFFICE
1967
PRICE 15*s.* 6*d.* NET

The Pressure-Drag due to Blunt Leading Edges on Two-Dimensional Aerofoils, at Transonic and Low-Supersonic Speeds

by W. J. GRAHAM

Reports and Memoranda No. 3465*
May, 1965

Summary.

Pressure drags, obtained from measured pressure distributions in the transonic and low-supersonic speed range, are compared for sharp and blunt leading-edged two-dimensional aerofoils. For the special blunt shapes considered here, the high pressures in the stagnation-point region are offset by low pressures generated further round on the leading edge and on the basic aerofoil itself. The result is that the changes in pressure drag due to blunting are small and in some cases favourable.

1. *Introduction.*

It is often assumed that the effect of blunting the leading edge of a sharp aerofoil section, or increasing the leading-edge size of an already blunt section, inevitably leads to an increase in wave drag at supersonic freestream speeds. Lighthill in Ref. 1 and the charts for estimating leading-edge wave drag in the Royal Aeronautical Society Data Sheets[2] both consider the effects of small leading-edge blunting. They conclude that increase in leading-edge size always results in increased drag and that the drag increments are substantial. Thus some efforts have been made to reduce leading-edge sizes, for supersonic flight, to the minimum proportions possible, although considerations of structural integrity, low-speed performance and heat transfer would have led towards the opposite extreme.

The drag of an aerofoil section comprises skin friction and pressure drag. The skin friction acts on the aerofoil through tangential forces and, although important in determining the total drag, it will not be considered further in this paper. The pressure drag acts on the aerofoil through pressures normal to the surface and, at Mach numbers above the critical value, is mainly wave drag, although a small part is due to the pressure out-of-balance caused by boundary-layer growth. In the present paper, attention will be focussed on the changes in surface (i.e. normal) pressure distribution by means of which the wave-drag changes are transmitted to the aerofoil. Changes in surface pressure resulting in a reduction of pressure drag must be compatible with a reduction of shock-wave strength in the flow field.

It is now known that at subsonic speeds an aerofoil section may produce a region of low pressure (just behind the stagnation-point region) which is effective in reducing the pressure drag when it acts on a forward-facing surface. This type of, so called, 'peaky' pressure distribution and its associated aerofoil geometry are discussed by Pearcey in Ref. 3. In this case, the low pressures in the 'peak' region are associated with a strong expansion wave which is generated by the surface and then reflected off the sonic line as a compression wave. This compression serves to reduce the strength of the shock which terminates the local supersonic region.

Following this subsonic experience, together with the known effects on blunted axi-symmetric bodies at supersonic speeds (*see* below), it is logical to enquire whether an aerofoil shape exists that will produce a similar low pressure region, which is effective in reducing pressure drag at supersonic speeds. A blunt leading edge produces a strong detached shock wave at supersonic speeds, but if the leading-edge geo-

* Replaces N.P.L. Aero Report 1151—A.R.C. 26 955.

metry generates a low pressure region the associated expansion wave may weaken the bow shock, well out in the flow field, and offset the high wave drag. Further, reflections of the expansion wave from the sonic line and bow shock may interact with the trailing shock to reduce its strength and again reduce the wave drag. At sonic free-stream speeds reflection of the expansion wave from the sonic line and subsequent weakening of the trailing-edge shock can be the only mechanism for reducing wave drag since no bow shock exists. The problem of blunting an axi-symmetric body has been studied extensively and it is now recognised that, under certain conditions of Mach numbers and geometry, a blunt nose may induce a low pressure region which is important in offsetting the high pressures in the stagnation region, so that the blunt shape has less wave drag than the sharp one. Traugott in Ref. 4 discusses the conditions for blunting a cone which lead to a low pressure region at the junction, throughout the supersonic and hypersonic range. Tests on hemispherically blunted cones and various power law bodies by Perkins, Jorgensen and Sömmer[5] show that, at supersonic speeds, the sharp axi-symmetric shape does not give minimum drag.

In order to explore the possibility of reducing aerofoil drag by the use of shapes which generate low pressure regions, the present investigation is a study of the pressure distributions and pressure drags of two geometrically simple, blunt aerofoil shapes relative to the sharp section from which they are derived. Measurements have been made through transonic to supersonic speeds to follow the development from subsonic to supersonic free streams.

The pressure measurements discussed in this Report were obtained as part of a broader investigation into the effects of leading-edge geometry on flows round aerofoils in the transonic and low-supersonic speed range. Only the results relevant to pressure drag have been extracted here. The other aspects are dealt with separately in Ref. 6.

2. *Wind Tunnel and Models*

The experiments were carried out in an N.P.L. transonic, induced-flow, wind tunnel which has a working section measuring 36 in. by 14 in. Slotted top and bottom liners (*see* Section 7) were used in the Mach number range 0·7 to 1·1, and solid liners for the Mach number of 1·4. The stagnation pressure was atmospheric, resulting in Reynolds numbers in the range 4·4 to $5{\cdot}0 \times 10^6$ per ft.

Pressures were measured on a multitube, mercury manometer.

The two-dimensional models were mounted spanning the 14 inch width of the tunnel. The basic section tested was circular-arc biconvex, described by radii of 30 in. and a chord of 10 in.; this model being designated R30. Blunted sections R3010 and R3015 were derived from the basic, sharp shape by leading edges of constant radii 0·10 in. and 0·15 in. respectively. The leading edge cylinders blend tangentially with the basic shape, giving chords somewhat less than 10 in. Details of the three aerofoil sections are given in Fig. 1.

The models were made by the 'tangent milling' method. In this a number of planes are cut tangent to the required contour, such that the point of intersection of any two adjacent planes deviates from the required shape by 0·0005 in. The final smooth shape is achieved by hand finishing. Static pressure holes were drilled normal to the surface, 0·010 in. diameter generally, but those near the leading edge were made 0·007 in. Forty pressure holes were used, distributed on the upper and lower surfaces.

No means of artificially fixing the model boundary-layer transition point was attempted.

3. *Accuracy of Measurements*

The main source of error in the measured data was indicated by the lack of agreement between pressures measured at points located symmetrically on the upper and lower surfaces of an aerofoil when set at the best choice of zero incidence, i.e. the incidence at which the pressure difference for each pair of symmetrically located holes was, on average, as small as possible. This assymmetry probably arose from irregularities in the tunnel flow and model shape.

The differences between the pressures on the two surfaces at zero incidence indicated that there was a possible error of about $\pm 0{\cdot}002$ in p/H_0, regardless of pressure level or position on the model. In calculating drag coefficients this gives an error of $\pm 0{\cdot}004$ in the pressure difference, $\Delta p/H_0$, of equation (1), leading to an error of about 0·01 in $C_{Dt/2}$, or 0·0005 in C_{Dc}.

Tunnel interference effects, which also influence the accuracy of the results, will be considered later, in Section 7.

4. *Pressure Distributions.*

Surface pressure distributions have been measured on the sharp section over the Mach number range 0·8 to 1·4, and on the two blunt sections over the range 0·7 to 1·4. The incidence range of 0 to 4 degrees was covered except for the highest Mach number, at which the flow could not be established on the blunt sections set above two degrees incidence.

Since we are here interested in drag, it is instructive to compare pressure distributions for the sharp and blunt sections plotted versus a thickness co-ordinate. A typical curve of this type is sketched in Fig. 2, where points corresponding to points on the aerofoil surface are indicated. The area within the loop formed by such a plot is proportional to the pressure-drag coefficient. Differences in pressure distributions looked at in this way then indicate changes in the pressure drag.

Measured pressure distributions for the sharp section, R30, and the blunt section with the larger leading-edge radius, R3015, are compared in Figs. 3 to 10. The surface pressure (p) is non-dimensionalised by the free-stream total-head (H_0). The thickness ordinate (z) is non-dimensionalised by the half-thickness ($t/2$), which is the same for all three sections. Thus the $2z/t$-ordinates for points common to both aerofoils (Fig. 1) are unchanged. When plotted in this way it can be readily seen if the pressures, in regions in which the aerofoils are unaffected in shape, are themselves affected by leading-edge blunting. The region in which the aerofoil shape is affected by blunting has the characteristic pressure distribution FAB (Fig. 2) between the suction peaks F and B that occur at the shoulders.

In discussing the pressure distributions those at a free-stream Mach number of 1·4 and at zero incidence (Fig. 9) will be considered first as they represent the clearest demonstration. It is immediately apparent that the main drag variations due to leading-edge blunting will arise from variations in pressure over the forward part of the aerofoil, since over the remainder the pressures are little affected by changes in leading-edge shape. At the leading edge of the sharp section the bow shock comes closest to being attached for any of the present tests. The stagnation region is very narrow; downstream of it the pressure falls rapidly to the sonic point and then continues monotonically towards the trailing edge. On the blunt shape the high pressures in the region of the stagnation point are spread over a larger forward facing area and, consequently, represent a drag increment. However, the flow round the leading edge expands rapidly through the sonic point and continues up to the sudden change of curvature at the shoulder, i.e. the point B in Fig. 2 at which the shape returns to that of the sharp aerofoil. At this point the pressure on the blunt section is over-expanded, in that it is substantially lower than at the same point on the sharp section. Downstream of the shoulder a rapid compression brings the pressure level on the blunt section back to that on the sharp section. This region of low pressure acts on a forward facing area of the surface, partly on the blunt leading edge (forward of point B in Fig. 2) and partly on the unmodified basic shape (behind point B), and so contributes a drag reduction. Schlieren photographs[6] show that the compression from the peak always involves a shock wave even though the surface pressure distributions are sometimes smooth.

The comparisons of pressure distributions for other Mach numbers at zero incidence (Figs. 3 and 6) are similar.

At incidence a further feature enters, namely, the expansion round the sharp leading edge produces a low pressure region on the upper surface. This is terminated by a rapid compression and the extent of the low pressure region in the z-direction is always appreciably less than for the blunt section. Furthermore, the pressure on the lower surface of the sharp section still falls monotonically, so that the low pressure region, still present for the blunt section, assumes added significance in reducing drag (*see* Fig. 10 for example).

As incidence is increased for the blunt section, two counteracting trends are noticed on the upper surface. Firstly, the lowest pressure, reached at the shoulder, falls and the pressure level immediately following is also reduced. This effect arises as the turning angle between the stagnation point and the shoulder increases and allows expansion to a higher local velocity. Secondly, the surface behind the shoulder becomes less inclined to the free-stream direction. On the pressure distributions this reveals itself as a contraction of the z-ordinate between the shoulder and crest. The former aerodynamic effect tends to decrease the pressure drag whilst the latter, geometric effect tends to increase it. Exactly converse trends are present on the lower surface.

For the blunt section at zero incidence and the lower range of Mach numbers, the pressure distributions in the vicinity of the shoulder indicate that a small boundary-layer separation bubble is present (Fig. 3). An increase of incidence or Mach number eliminates the small region of constant pressure and appears to suppress the separation.

The pressure distributions for the other blunt section, R3010, follow a similar form to those for R3015. A typical comparison is made in Fig. 11, for a free-stream Mach number of 1·0 and incidence of 2 degrees. The pressure reached at the shoulder is not so low in the case of R3010 since the surface slope at that point is greater than for R3015 : the turning angle from the stagnation point is less. The scale of the R3010 leading edge in the z-direction is less since the leading-edge radius is a smaller fraction of the maximum thickness.

It is observed that at Mach numbers of unity and above there is a rise in pressure, before the trailing edge is reached, which would not be expected in an inviscid flow. At a Mach number of one the terminating shock has probably not moved right on to the trailing edge and certainly not adopted the oblique form appropriate to supersonic downstream flow. The resulting pressure distribution in this region is therefore strongly affected by shock-wave boundary-layer interaction and possibly by separation. Some smoothing of the pressure jump through the trailing shock due to this interaction remains at the Mach number of 1·4. On the blunt section this interaction is more marked than for the sharp section (e.g. Figs. 6 to 8), resulting in locally higher pressures (now on rearward facing areas) which could in themselves make the pressure drags of the former sections low compared with the latter. However, this effect is an indirect consequence of the blunting, through the medium of the boundary layer, and is Reynolds number dependent. It would certainly be diminished at the higher Reynolds numbers of flight conditions. This effect has therefore been eliminated from the comparisons. Following Ref. 7, the pressures near the trailing edge have been obtained by extrapolating the pressures upstream of the interaction, assuming simple-wave expansion. The modified pressures are shown as a dotted line in Figs. 6 to 11.

5. *Pressure Drags.*

A pressure drag coefficient may be calculated by integration of the pressure distribution using

$$C_D = \frac{2H_0}{\gamma p_0 M_0^2} \int_{z/l\,\min}^{z/l\,\max} \Delta\left(\frac{p}{H_0}\right) d\frac{z}{l}, \tag{1}$$

where Δ denotes the difference between values of pressure at a given value of z/l. The resulting drag coefficient is based on the length l, used to form the non-dimensionalised thickness ordinate, z/l. Using the measured pressure distributions, values of pressure drag coefficient have been obtained for the sharp and two blunt sections over the range of Mach number and incidence. The effects of shock-wave boundary-layer interactions at the trailing edge, for free-stream Mach numbers of unity and above, have been eliminated by the method described in the previous section.

The drag coefficients obtained from plots of p/H_0 versus $2z/t$ (such as Figs. 3 to 11) are based on the half-thickness, $t/2$, which is the same for all three sections. The drag variations with Mach number are shown in Figs. 12 to 14 for incidences of 0, 2 and 4 degrees respectively. The drag variations with incidence are shown in Fig. 15 for Mach numbers 0·80, 1·00 and 1·40.

For the type of leading-edge blunting considered here, the greater the degree of blunting the smaller is the chord of the section, so that the three sections have different thickness-chord ratios. Thus Figs. 12 to 15 compare drags of sections having different thickness-chord ratios. Since thickness-chord ratio is an important parameter in aerofoil section design (from both aerodynamic and structural considerations) it is desirable to compare drags of sharp and blunt sections having equal values of this quantity. The transonic similarity law, as given in Ref. 8, enables the measured drags on the sharp section, R30, to be factored to obtain drags appropriate to sharp sections of the same thickness-chord ratios as either of the two blunt sections. According to this law the drag coefficient, $C_{D_{c2}}$, of a section of thickness τ_2 at a Mach number M_2 is related to the drag coefficient, $C_{D_{c1}}$, of a section of different thickness τ_1 and at a Mach number M_1 by

$$C_{D_{c2}} = C_{D_{c1}} \left[\frac{(\gamma+1)M_1^2}{(\gamma+1)M_2^2}\right]^{1/3} \left(\frac{\tau_2}{\tau_1}\right)^{5/3}, \tag{2}$$

where M_1 and M_2 are related through the transonic similarity parameter, ξ, which is given by

$$\xi_0 = \frac{1-M_1^2}{[(\gamma+1)\tau_1 M_1^2]^{2/3}} = \frac{1-M_2^2}{[(\gamma+1)\tau_2 M_2^2]^{2/3}}. \tag{3}$$

The Mach numbers for which the estimated sharp-section drags apply are thus given by equation (3) and are slightly different from the corresponding Mach numbers at which the R30 drags were measured, except for the case where the test Mach number is 1·0 and $M_2 \equiv M_1$.

Fig. 16 shows the drag variation with Mach number for the two blunt sections at zero incidence compared with estimated drags for sharp sections of the same thickness-chord ratios, obtained as indicated above. These drag coefficients are now based on section chord (c).

If incidence is regarded as producing a change in surface co-ordinates it may be treated in the same way as thickness. Then the transonic similarity law can be applied to the measured drags on section $R30$, at incidence, to obtain drags on sharp sections of different thickness. In this case incidence will be changed in the same ratio as the change in section thickness, and the appropriate free-stream Mach number will be slightly different, as in the zero incidence case.

The variation of drag coefficients (based on chord) with incidence at Mach numbers of 0·80, 1·00 and 1·40, for the two blunted sections, $R3010$ and $R3015$, are compared in Figs. 17 and 18 respectively with estimated drags of sharp sections of the same thickness-chord ratios.

Pressure distributions on biconvex aerofoil shapes have previously been measured by Michel, Marchaud and Le Gallo[7], Henshall and Cash[9] and Kawamura and Karashima[10]. The latters' results have not been corrected for shock-wave boundary-layer interaction at the trailing edge and insufficient detail is given to perform the modification. Results from the other sources have been used to derive drags and are compared with the present $R30$ results at zero incidence in Fig. 19, as a variation of reduced pressure-drag coefficient ($\bar{C}_{D_c}$) with the similarity parameter (ξ_0); where $\bar{C}_{D_c}$ is given by

$$\bar{C}_{D_c} = C_{D_c} \frac{[M_0^2(\gamma+1)]^{1/3}}{\tau^{5/3}}, \tag{4}$$

and ξ_0 is given by equation (3). Also shown is the theoretical pressure-drag coefficient obtained in Ref. 8.

6. *Discussion of Drags.*

The drag variations with Mach number and incidence are of very similar form for both the sharp and blunt sections. The drag coefficient is low at the low end of the Mach number range, but increases rapidly as Mach number is increased towards unity (*see* Figs. 12, 13 and 14). This drag rise is associated with the rapid rearward movement of shock waves on the upper and lower surfaces. The maximum drag coefficient occurs close to a free-stream Mach number of one; beyond this it falls slowly.

For low incidences the drag coefficient varies only slowly with incidence (Fig. 15). The sharp section drag always increases with increasing incidence, but in some cases the drags of the blunt sections initially decrease slightly as incidence is raised above 0 degrees. For incidences above about 2 degrees the drags of the blunt sections tend to increase more rapidly with incidence than for the sharp section. The counteracting trends mentioned in Section 4 are evidently behaving in such a way that, as incidence is raised, the increased suction due to the decreasing pressures in the peak region initially gains over the effect of reducing the local surface slopes, whereas at higher incidences the converse applies. A further, small effect tending to increase the drag at small incidence, for subsonic Mach numbers, is the presence of the local separation at the shoulder, which prevents the full development of the low pressures in the peak region. As pointed out in Section 4, this separation is not present at higher incidences.

The differences between the measured pressure-drag coefficients (based on $t/2$) for the sharp section and the blunt sections are shown in Fig. 20, for incidences of 0, 2 and 4 degrees over the Mach number range 0·80 to 1·40. For the section R3010, which has the smaller degree of blunting, there exists an intermediate range of Mach number for which the drag is actually less than for the sharp section (Fig. 20a). For the section R3015 the drag is always more than the drag of the sharp section, but at 2 degrees incidence the increment becomes insignificant near to 0·95 Mach number (Fig. 20b). For both sections the drag increment varies with incidence. There appears to be no simple correlation between drag increment and leading-edge radius.

Holder and Chinneck[11] measured pressure distributions on blunted flat plates at Mach numbers from about 1·4 to 1·8. With this work as a basis much has since been inferred as to the effect, on pressure drag, of blunting two-dimensional aerofoil shapes at supersonic speeds. In Lighthill's discussion in Ref. 1, on the flow about slightly blunted aerofoil shapes at supersonic speeds, he suggests that the low pressures, if any, induced by the blunt leading edge have only a small and insignificant effect on the pressure drag, and that incidence effects are unimportant. The two simple, blunt leading edges on sections R3010 and R3015 do produce marked regions of low pressure, throughout the Mach number range. The pressure distributions (Figs. 3 to 11) show that these low pressures are likely to have a significant effect in offsetting the drag due to the high pressures on the leading edge itself. In the Royal Aeronautical Society Data Sheets[2] basic data from measurements on circular cylinders[12] and cylindrically blunted flat plates[11] have been collected and used to give drag increments due to small cylindrical leading edges on arbitrary aerofoil shapes, at supersonic speeds and zero incidence. Like Ref. 1, the Data Sheets diminish the importance of the induced pressures and any negative drag contributions arising from them. In addition the procedure suggested in Ref. 2 fails to account for the drag due to a sharp leading edge. That this is of the same order as the drag of a blunt leading edge at low supersonic speeds can be seen from the pressure distributions (Figs. 6 to 11).

The zero incidence drag increments, at supersonic speeds, for the sections R3010 and R3015 as calculated by following Ref. 2 are shown in Fig. 20. It is evident that the drags due to leading edges of the type being considered here are considerably overestimated. The pressure distributions of Refs. 12 and 11, forming the basis of Ref. 2, agree closely with those measured on the cylindrical leading edges of R3010 and R3015, and any differences do not account for the incremental drag discrepancy in Fig. 20.

There is no fundamental difference between the drag producing mechanisms for small leading edges, as considered in Refs. 1 and 2, and large leading edges, as on the sections tested here: only the scale of the drag increments differs. If the drag contribution of a blunt leading edge, however small, is required to any accuracy, so that the leading edges of different geometries can be compared, then all the drag contributions indicated here must be accounted for.

As free-stream Mach number is increased the region of low pressure induced by the leading edge would be expected to diminish, since the pressure level on the sharp shape itself becomes low. The applicability of the procedures of Ref. 1 and 2 are then expected to improve at high Mach numbers.

When the pressure drags of the blunt sections are compared with the drags of sharp sections having the same thickness-chord ratios (Figs. 16, 17 and 18) the blunt sections are seen in a more favourable light. It is found that significant ranges of Mach number and incidence exist for which both the blunt sections have less drag than the corresponding sharp sections.

It is shown in Fig. 19 that the pressure drags of R30 agree closely with those for the 4 per cent thick, bi-convex section of Ref. 9. The same wind tunnel was used for both sets of tests. These N.P.L. data lie consistently above those of Ref. 7, in which pressure measurements were made on a circular-arc bump on a wind tunnel wall. This configuration has no stagnation point, so that the pressures near the leading edge are substantially lower, and the drag consequently less, than for the complete section tested here. Comparison of the pressure distributions shows, also, that in the region of $\xi_0 = -0{\cdot}6$ ($M_0 \approx 0{\cdot}9$) the shocks on R30 lie some 10 per cent further back, an effect probably due to smaller tunnel interference in the present case (*see* Section 7). This difference in shock position accounts for the particularly large differences in drag in this region.

7. *Tunnel Interference Effects.*

The results at the supersonic Mach number of 1·4 are free from any tunnel interference effects since the model lies within the diamond formed by the bow shock and its reflection from the walls. At the very low supersonic speeds the local pressures are 'frozen' (i.e. nearly independent of free-stream Mach number) and therefore not greatly affected by tunnel interference, the main influence in this case being to alter the effective free-stream Mach number.

At subsonic speeds the results would be subject to significant tunnel interference effects due to both classical blockage and lift-interference, the latter being predominantly due to the downwash effects appropriate to an open-jet configuration.

In the transonic speed range between these two régimes a mixture of the two situations occurs. In the local supersonic flow upstream of the shocks the local pressures tend to be uninfluenced by the walls, especially when they have reached their sonic-range 'freeze' values. In the subsonic flow downstream, however, the blockage effects, at least, still apply and particularly the position of the terminating shock is still influenced by the wall configuration.

In Ref. 13, Pearcey, Sinnott and Osborne considered these interference effects and drew attention also to a distortion of the local supersonic flow that could occur prior to the sonic 'freeze', if the open area of the slotted walls is too large. Their main discussion concerns measurements in an N.P.L., 20 in. by 8 in. working-section tunnel, but some results are included for the 36 in. by 14 in. tunnel used here. The liners normally used in this tunnel are 0·091 open-area ratio and give effectively 'open jet' results. The slotted-wall parameter, T, of Meader and Wood[14] equals 0·96 in this case (*see* table in Fig. 21). This parameter involves slot spacing, tunnel height and open-area ratio and defines the wall characteristics explicitly. According to Ref. 13, closing all but three of the eleven slots in each liner gives nearly zero-interference walls ($\sigma = 0{\cdot}025$, $T = 0{\cdot}73$). The more open walls are normally used since they allow operation at higher Mach numbers.

Further, unpublished results are available for tests on a 5 in. chord, RAE 104 section in the 36 in. by 14 in. tunnel with various degrees of wall open area. A typical variation of pressure (at 0·52 chord) with free-stream Mach number is shown in Fig. 21 for different open-area ratios. The maximum Mach number attainable with the liners 0·025 open was 0·93, but Mach numbers up to nearly 1·1 were possible with an open area of 0·042. At Mach numbers above about 0·9, for which the sonic 'freeze' has been reached locally, varying the wall open-area has little effect on the model surface pressures; the change in p/H_0 being less than 0·010. From the trend of the curves one might reasonably conclude that if the tunnel would run with 0·025 open area the effects on pressure would likewise be very small. At Mach numbers below 0·9, for which the pressures vary substantially with Mach number, the interference effects are appreciable: the maximum deviation between the curves for open areas of 0·025 and 0·091, which occurs near $M_0 = 0{\cdot}8$, is about 0·025 in M_0. The section shapes considered in this Report are twice the chord of the R.A.E. section and show a rather different type of pressure distribution. It was, therefore, necessary to check the interference effects in the present cases.

Limited tests were carried out using models R30 and R3015, with an open-area ratio of 0·025. The variation of pressure with Mach number, at two fixed stations, is shown in Fig. 22 for section R3015 at 2 degrees incidence. The maximum Mach number attainable with the liner slots in this partially closed condition was about 0·9. The upper curves in Fig. 22 are for $x/c = 0{\cdot}014$ and are representative of the behaviour in the low pressure region near the shoulder. The pressures in this region reach sonic 'freeze' near to $M_0 = 0{\cdot}8$ and are thereafter unaffected by wall configuarion. Further back, at $x/c = 0{\cdot}442$, the pressures 'freeze' at a higher Mach number, near to 0·9, as is shown in the lower pair of curves in Fig. 22. The behaviour in this region is similar to that found previously for the RAE 104 section and we might infer that at higher Mach numbers the pressures are similarly little affected by wall configuration. The tunnel wall opening has a marked effect on the position of the rear shocks, the shocks moving towards the trailing edge as liner slots are progressively closed. Tests on section R30 showed the same dependence on Mach number and wall configuration as those of R3015.

The comparative tests made here, taken with previous results in the same tunnel, indicate that where the pressures are 'frozen' with respect to free-stream Mach number in the normal ($\sigma = 0{\cdot}091$) tunnel configuration they do not suffer from significant wall interference effects. Thus for Mach numbers above 0·8 the values of pressure in the region of the leading edge are free from interference errors. For Mach numbers above 0·9 the pressure changes induced by the blunt leading edges are unaffected by interference effects since they occur forward of the rear shocks and are 'frozen'. The drag differences presented here for Mach numbers above 0·9 should, therefore, be not subject to appreciable errors. The absolute values of drag up to sonic velocity are highly dependent on rear shock position and, therefore, greatly affected by tunnel interference. It is this effect which could account for the differences between the N.P.L. results and those of Ref. 7 which are evident in Fig. 19. For Mach numbers of unity and above, for which the rear shock is at the trailing edge, no significant error due to wall interference is present.

8. *Theoretical Prediction of Surface Pressures.*

Any theoretical approach to obtaining the flow field around aerofoils, such as those tested here, at transonic and supersonic Mach numbers, is made complex by the presence of subsonic and supersonic regions and the resulting mixed elliptic-hyperbolic nature of the basic equations.

In the high subsonic Mach number régime an aerofoil produces a region of supersonic flow embedded within the mainly subsonic flow field. A theoretical approach must at the same time take into account the whole flow field. In general, shock waves will be associated with the supersonic flow region and their presence would seem to preclude any general solution at the present time. A method for calculating flows around aerofoils with local supersonic regions, but without shock waves, is being developed by Nieuwland[15], using the hodograph technique.

The particular case of slender aerofoils at zero incidence and Mach numbers very close to unity has been treated by Spreiter and Alksne[8] using a small perturbation approximation. The pressure distribution obtained is compared with that measured on the sharp section, R30, in Fig. 23. The agreement between theory and experiment, particularly over the forward part, is good. Randall[16] has extended this method for use with round-nosed aerofoils and has achieved good general agreement with experiment in certain cases, even though the prediction of sonic point is unsatisfactory. However, the theory breaks down unless local velocity is increasing and thus Randall's method is inapplicable in our present case, where the compression after the leading edge is an essential feature of the flow.

At supersonic Mach numbers the problem becomes somewhat easier because the flow field can be dealt with as a number of independent regions. In the special case of a sonic free-stream the flow field about the forward part of a circular cylinder, with axis normal to the stream direction, has been computed from the complete, inviscid equations by Chuskin[17] after setting them in suitable form by the use of Dorodnitsyn's method of integral relations[18]. This solution is applicable to any two-dimensional shape, such as the cylindrical leading edge of an aerofoil, providing it is of constant radius up to, or beyond, the limiting characteristic. In Chuskin's solution this leaves the surface where the slope is 12·5 degrees so the result should be applicable to the present, blunt leading edges. The pressure distribution on a circular cylinder, obtained from Ref. 17, is shown in Fig. 23, plotted in terms of the section co-ordinate $2z/t$. Also shown

in Fig. 23 are pressures measured on the leading edge of the blunt section R3015 and these are seen to be in good agreement with theory. The relationship $p/H_0 = \sin\theta$ (where θ is the surface slope) is found to represent the pressures quite well up to surface slopes of about 15 degrees and is plotted in Fig. 23.

Chushkin's method can be applied to obtain the pressure distribution on any convex, symmetrical leading-edge shape. If one takes this solution with the sharp aerofoil solution mentioned earlier, one can get some way towards predicting the pressure distribution on a blunt leading-edged aerofoil at sonic velocity, bearing in mind that the pressure returns to its sharp leading-edge distribution sufficiently far behind the blunt leading edge (Section 4). The problem of joining the pressure distributions remains and if, as in the cases tested here, a compression involving shock waves follows the leading edge flow, then no method is available. If, however, the flow behind the leading-edge does not involve shock waves then it can be computed by using a characteristic network or a continuation of the integral relations method.

At higher, supersonic Mach numbers the problem of finding the pressures on an aerofoil shape can be approached in a similar manner. The flow round the blunt leading edge can be solved again by application of Dorodnitsyn's method and several examples have been calculated by Belotserkovskii[19] and Belotserkovskii and Chushkin[20]. There is a dearth of information between Mach numbers of one and two as, apparently, computational problems arise. As before, the solution to the transonic problem at the blunt leading edge can be extended downstream using characteristics or the integral relations method, but either approach will break down if shock waves are generated. The asymptotic pressure level can again be calculated from the sharp-section values. The sharp leading edge case becomes more straightforward at Mach numbers where the bow shock is attached. The pressures on section R30 have been calculated using simple wave theory for the Mach number at which the flow behind the attached bow shock is just sonic ($M_0 = 1{\cdot}42$). These are shown relative to measured values at a Mach number of 1·40 in Fig. 24. Again the simple 'sin θ' relationship expresses the leading-edge pressures quite well if written in the form $p/p_s = \sin\theta$, where p_s is the stagnation point pressure.

9. *Conclusions.*

The pressure drags of the two-dimensional sections formed by cylindrical blunting of the leading edge of a circular-arc, biconvex section have been measured and compared with the pressure drag of the basic shape, in the transonic and low supersonic Mach number range. The drag increments due to the blunt leading edges vary with both free-stream Mach number and incidence. The small drag changes resulting from the blunting are associated with the low pressure region induced by the over-expansion around the leading-edge cylinder. This low pressure acts on forward facing areas of the surface to give a negative drag component. Sufficiently far back from the leading edge the pressure distribution becomes independent of leading-edge shape.

At sonic free-stream Mach number, the pressures on the sharp leading-edged section and on the leading edges of the blunt sections are in good agreement with theory.

Previously accepted methods of predicting the effect of blunt leading edges on aerofoil drag, at supersonic Mach numbers, seriously overestimate the drag penalties in the low supersonic range.

When the drags of the blunt sections are compared with those for sharp sections of the same thickness-chord ratios, it is found that there is an appreciable part of the Mach number and incidence ranges for which the blunt leading edges cause no significant increase, and even slight reductions, in pressure drag.

The relative drags, or drag differences, for the three sections tested are not subject to significant wind-tunnel interference effects above a Mach number of 0·9, although the absolute values of drag are liable to large interference errors up to sonic velocity. The drags at Mach numbers above 1·0 have no significant interference errors.

From the present limited results the following general conclusions can be drawn:

1. The radius, by itself, does not determine the drag due to a leading edge.
2. The low pressure region at the junction between the leading-edge and the remainder of the aerofoil plays an important part in affecting the drag and, therefore, the section geometry in this region is important.

3. A sharp leading-edged aerofoil does not give the minimum pressure drag of all sections of the same thickness-chord ratio.

The blunt sections which have been tested were chosen for their simple geometry and are not necessarily optimum from the drag point of view. It appears, from the pressure distributions, that it should be possible to extend the low pressure region, which follows the expansion on the leading edge cylinder, by some suitable modification to the surface in that region, so making the low pressure region more effective in reducing drag.

In normal applications it would be necessary to reconcile the advantages of a blunt leading edge, such as that tested here, with reasonable subsonic performance. The present shapes, at low speeds, would have high local velocities followed by boundary-layer separation at the shoulder. A practical design would require a less rapid change of curvature in the region of the shoulder, in the hope of alleviating the local separation effects. Further work is necessary in order to develop such a shape.

10. *Acknowledgements.*

Acknowledgement is due to Miss B. Redstone, Miss A. G. J. MacDonald and Mr. P. Squire for carrying out most of the experimental work and, together with Miss S. Woolgar and Miss J. Soulsby assisting with the data reduction. Mr. K. Watson and Mr. J. Parker made the wind-tunnel models.

LIST OF SYMBOLS

M	Mach number
p	Pressure
H_0	Total pressure
x, z	Co-ordinates defined in Fig. 2
c	Section chord
t	Section thickness
τ	Section thickness-chord ratio, $= t/c$
γ	Ratio of specific heats
ξ_0	Transonic similarity parameter, $= \dfrac{1-M_0^2}{[(\gamma+1)\tau M_0^2]^{2/3}}$
C_D	Pressure-drag coefficient
$\bar{C}_D$	Reduced pressure-drag coefficient, $= \dfrac{C_D[M_0^2(\gamma+1)]^{1/3}}{\tau^{5/3}}$
θ	Surface slope
$2l$	Distance between centrelines of adjacent liner slots
h	Tunnel height
σ	Tunnel wall open-area ratio
C	$-\dfrac{2l}{\pi} ln \sin \dfrac{\pi\sigma}{2}$
T	Tunnel slotted-wall parameter, $= \dfrac{1-C/h}{1+C/h}$

Subscripts

o	Free-stream values
s	Stagnation-point values
c	Denotes drag coefficient based on chord
$t/2$	Denotes drag coefficient based on half-thickness.

REFERENCES

No.	*Author(s)*	*Title, etc.*
1	M. J. Lighthill	*General theory of high speed aerodynamics.* ed., W. R. Sears. High speed aerodynamics and jet propulsion Vol. VI pp. 416–425. 1955. Oxford University Press.
*2	. . . . .	Roya, Aeronautical Society Data Sheets. Aerodynamics S.02.03.05. 1954.
3	H. H. Pearcey	The aerodynamic design of section shapes for swept wings. *Advances in Aeronautical Sciences.* Vol. 3. Proceedings of 2nd International Congress in the Aeronautical Sciences, Zürich 12–16 September, 1960. Pergamon Press.
4	S. C. Traugott	Some features of supersonic and hypersonic flow about blunted cones. *J. Aero-Space Sciences*, Vol. 29, pp. 389–399. 1962.
5	E. W. Perkins, L. H. Jorgensen and S. C. Sommer	Investigation of the drag of various axially symmetric nose shapes of fineness ratio 3 for Mach numbers from 1·24 to 7·4. NACA Rpt. 1386. 1958.
6	W. J. Graham	The flow about a family of simple, blunt, and sharp leading-edged, two-dimensional aerofoils at transonic and low supersonic speeds. N.P.L. Aero Report 1189. February, 1966. A.R.C. 27838.
7	R. Michel, F. Marchaud and J. Le Gallo	Étude des Écoulements Transsoniques Autur de Profils Lenticulaires, a Incidence Nulle. O.N.E.R.A. Publication 65, 1953.
8	J. R. Spreiter and A. Y. Alksne	Thin airfoil theory based on approximate solution of the transonic flow equation. NACA Report 1359, 1958.
9	B. D. Henshall and R. F. Cash	Unpublished N.P.L. data on a two-dimensional, 4% thick, biconvex aerofoil at transonic speeds.
10	R. Kawamura and K. Karashima . .	Experimental investigation of transonic flow past two-dimensional biconvex circular-arc airfoils at small angles of attack. University of Tokyo *Aero. Research Inst.*, Rpt. No. 342. April, 1959.
11	D. W. Holder and A. Chinneck	The flow past elliptic-nosed cylinders and bodies of revolution in supersonic air streams. *Aeronaut. Q.* Vol. IV, pp. 317–340. 1954.
12	F. E. Gowen and E. W. Perkins	Drag of circular cylinders for a wide range of Reynolds numbers and Mach Numbers. NACA T.N. 2960. June, 1953.

---

* This Data Sheet has now been withdrawn from circulation. It has been replaced by Wings SO2.03.10, Aug. 1964, which gives, correctly, the wave drag of blunt flat-plates at zero incidence.

REFERENCES—*continued*

No.	*Author(s)*	*Title, etc.*
13	H. H. Pearcey, C. S. Sinnott and J. Osborne	Some effects of wind tunnel interference observed in tests on two-dimensional aerofoils at high subsonic and transonic speeds. AGARD Rpt. 296. March, 1959.
14	P. F. Maeder and A. D. Wood	Transonic wind tunnel test sections. *Z.angew. Math. Phys.* Vol. VII, pp. 177–212. 1956.
15	G. Y. Nieuwland	The computation by Lighthill's method of transonic potential flow around a family of quasi-elliptical aerofoils. *National Aero- and Astronautical Research Institute*, Holland. NLR-TR T. 83. September, 1964.
16	D. G. Randall	Transonic flow over two-dimensional round-nosed aerofoils. A.R.C. C.P. 456. September, 1958.
17	P. I. Chushkin	Calculation of certain sonic flows of a gas. Translated by J. W. Palmer. R.A.E. Library Translation 816. 1959.
18	A. A. Dorodnitsyn	A method for the numerical solution of certain non-linear problems of aerohydrodynamics. *Transactions of the 3rd All-Union Mathematical Conference*, Vol. 2. 1956.
19	O. M. Belotserkovskii ..	Flow with a detached shock wave about a symmetric profile. *Journal of Applied Mathematics and Mechanics* (P.M.M.), Vol. 22, pp. 279–296. 1958.
20	O. M. Belotserkovskii and P. I. Chushkin	Supersonic flow past blunt bodies. *Archiwum Mechaniki Stosowanej.* Vol. 14, pp. 461–490. 1962.

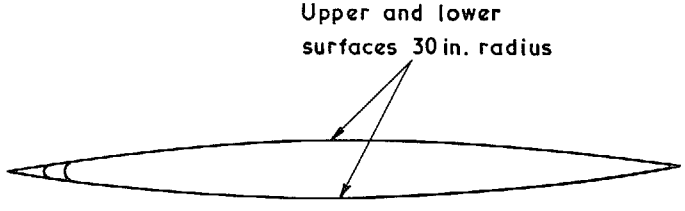

Model designation	L.E. radius	Chord	t/c
R 30	0 in.	10·00 in.	0·0839
R 3010	0·10 in.	9·46 in.	0·0887
R 3015	0·15 in.	9·15 in.	0·0917

FIG. 1. Description of sections for two-dimensional models.

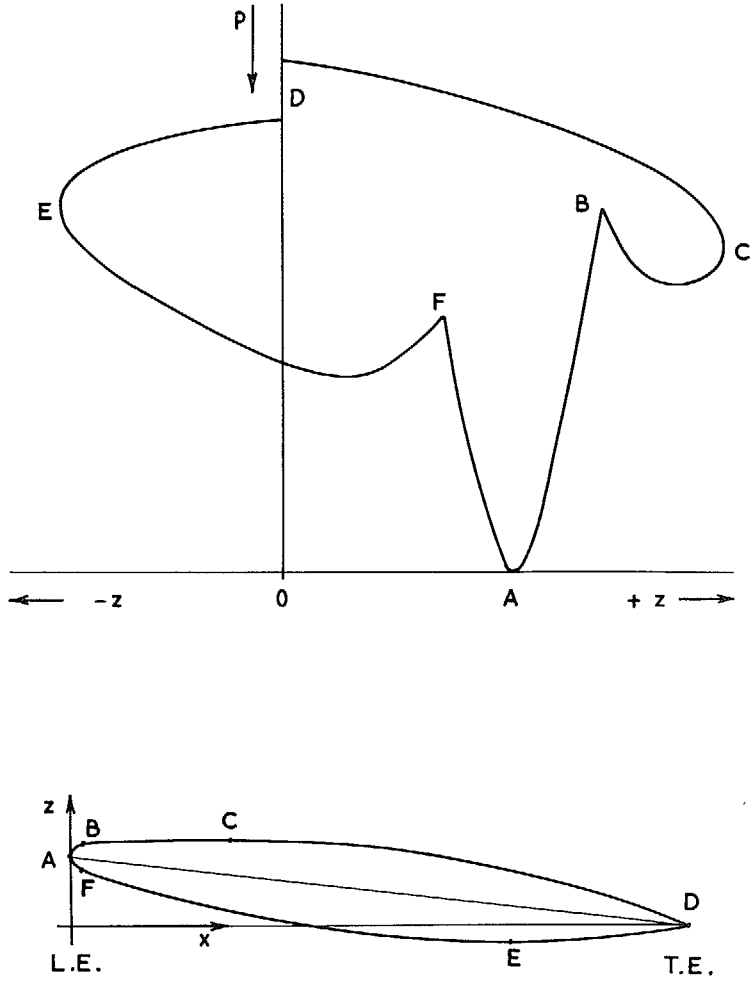

FIG. 2. Sketch of pressure distribution versus thickness co-ordinate, showing correspondence with points on aerofoil surface.

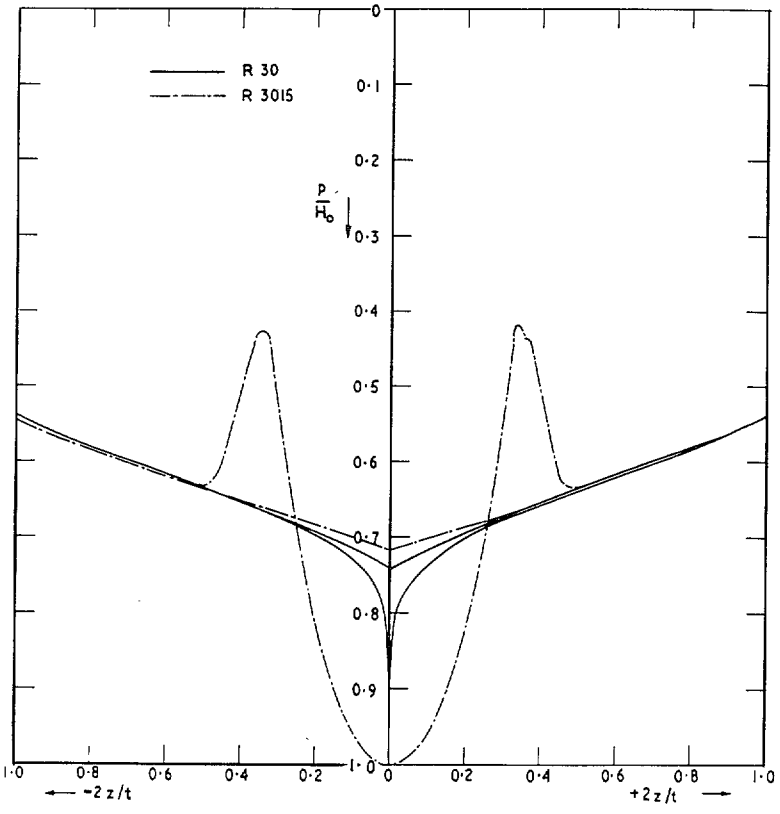

FIG. 3. Comparison of pressure distributions on sections R30 and R3015: $M_0 = 0{\cdot}80$, $\alpha = 0^0$.

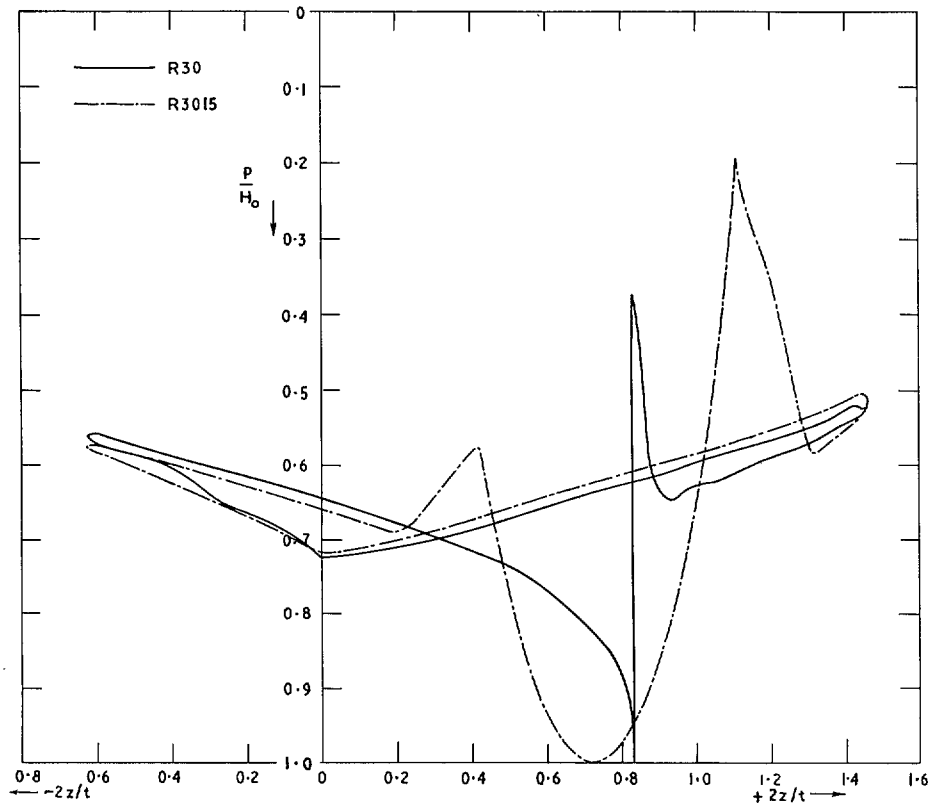

FIG. 4. Comparison of pressure distributions on sections R30 and R3015: $M_0 = 0{\cdot}80$, $\alpha = 2^0$.

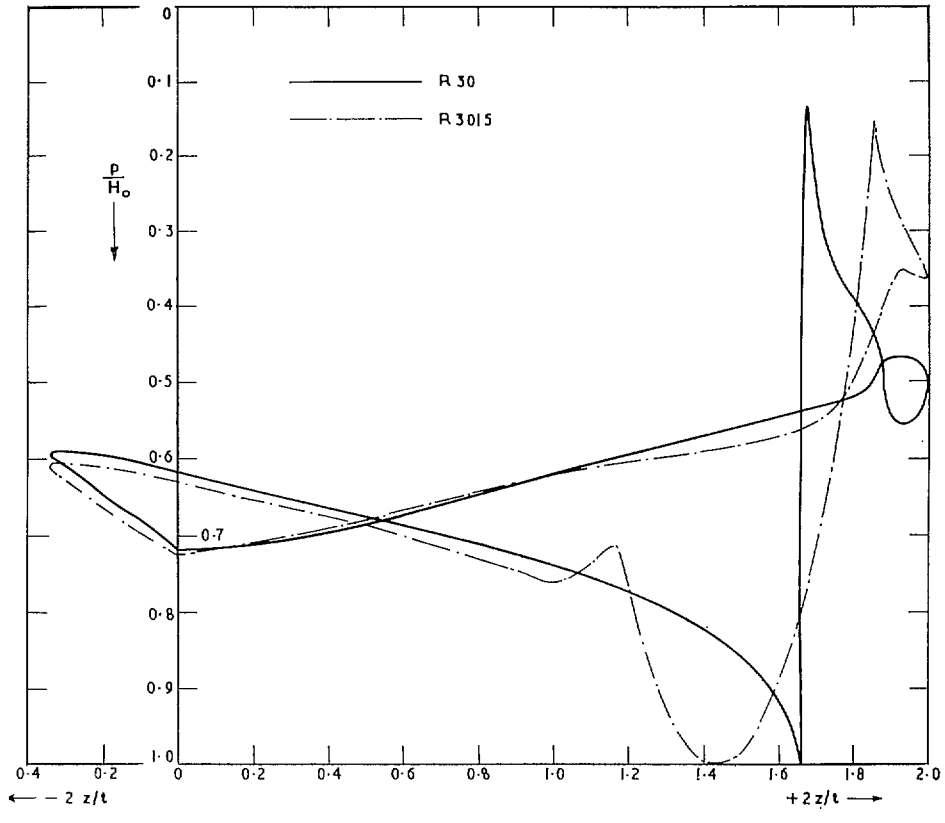

FIG. 5. Comparison of pressure distributions on sections R30 and R3015. $M_0 = 0{\cdot}80$, $\alpha = 4^0$.

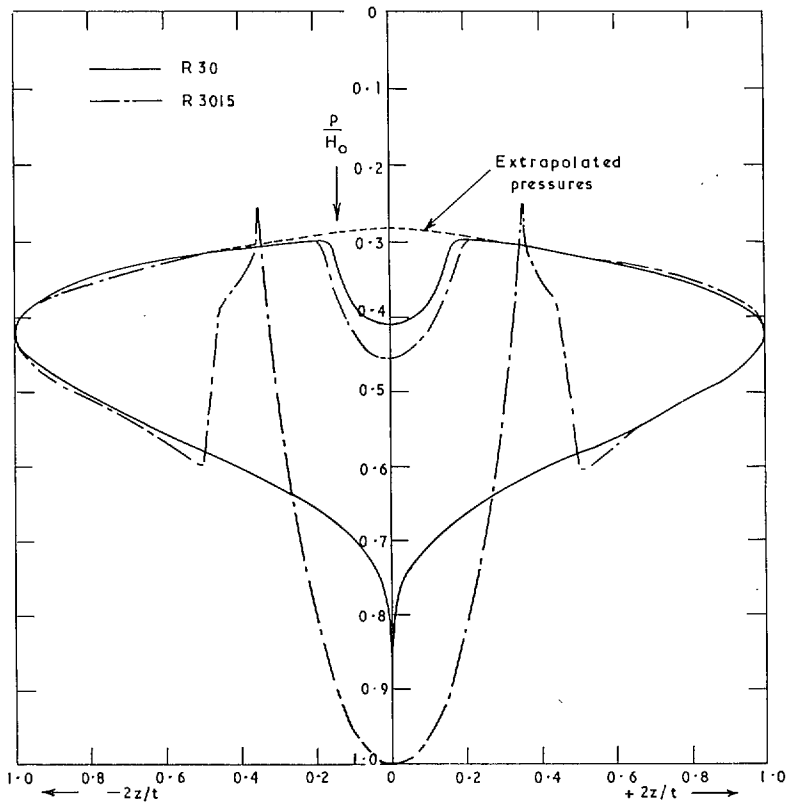

FIG. 6. Comparison of pressure distributions in sections R30 and R3015. $M_0 = 1{\cdot}00$, $\alpha = 0^0$.

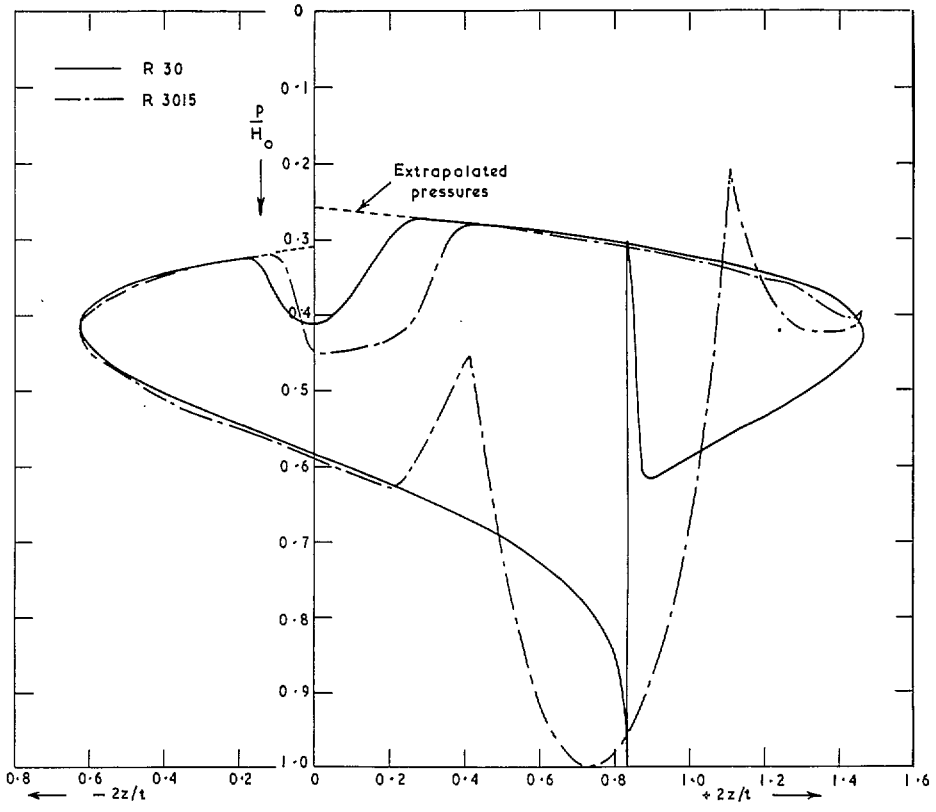

FIG. 7. Comparison of pressure distributions on sections R30 and R3015. $M_0 = 1{\cdot}00$, $\alpha = 2^0$.

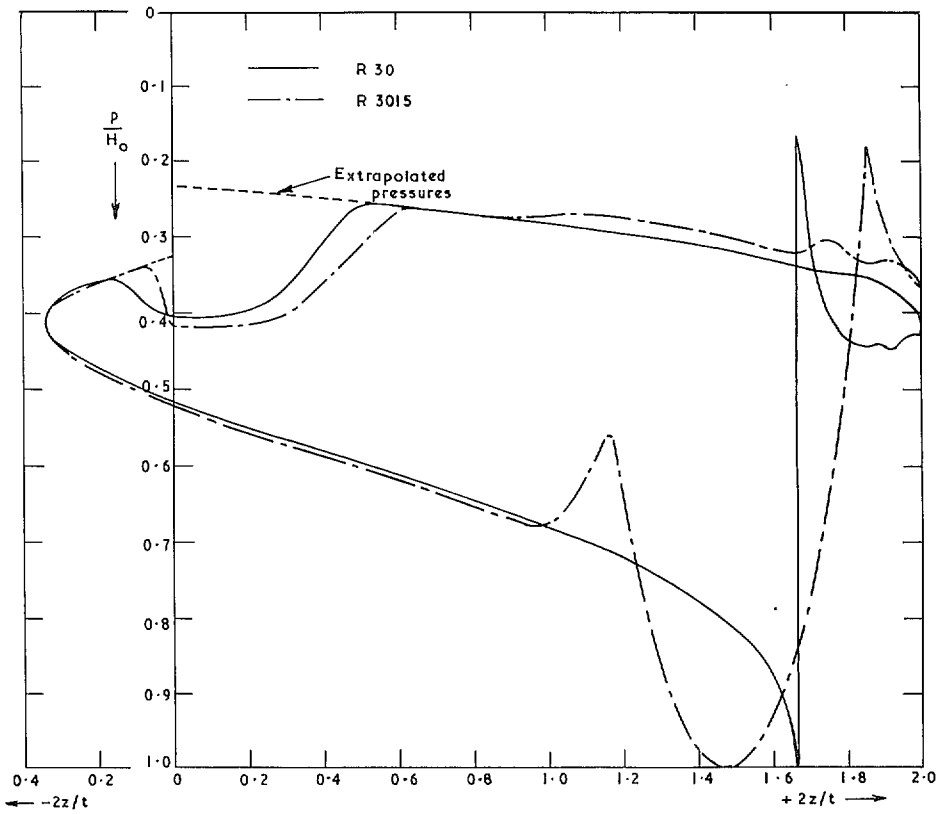

FIG. 8. Comparison of pressure distributions on sections R30 and R3015. $M_0 = 1{\cdot}00$, $\alpha = 4^0$.

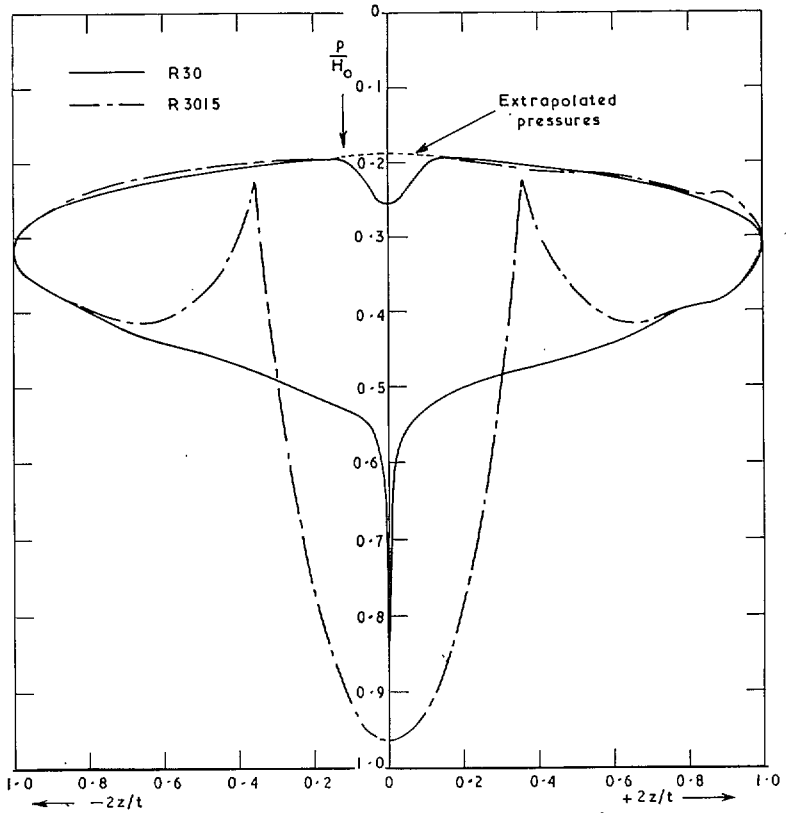

FIG. 9. Comparison of pressure distributions on sections R30 and R3015. $M_0 = 1{\cdot}40$, $\alpha = 0^0$.

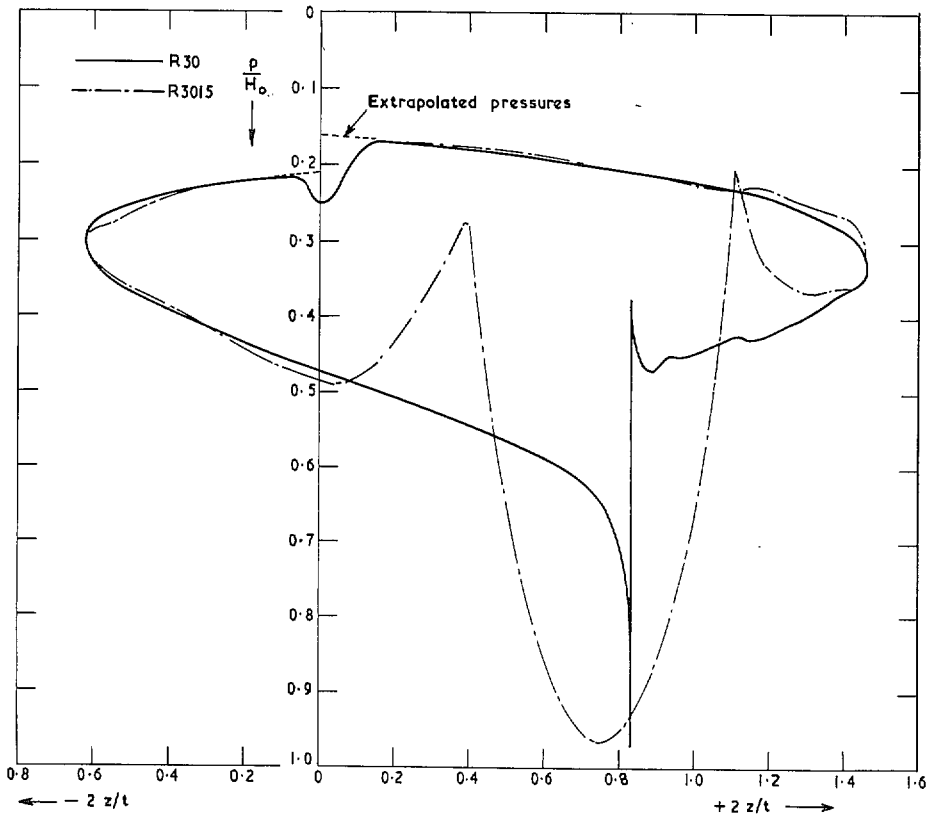

FIG. 10. Comparison of pressure distributions on sections R30 and R3015. $M_0 = 1{\cdot}40$, $\alpha = 2^0$.

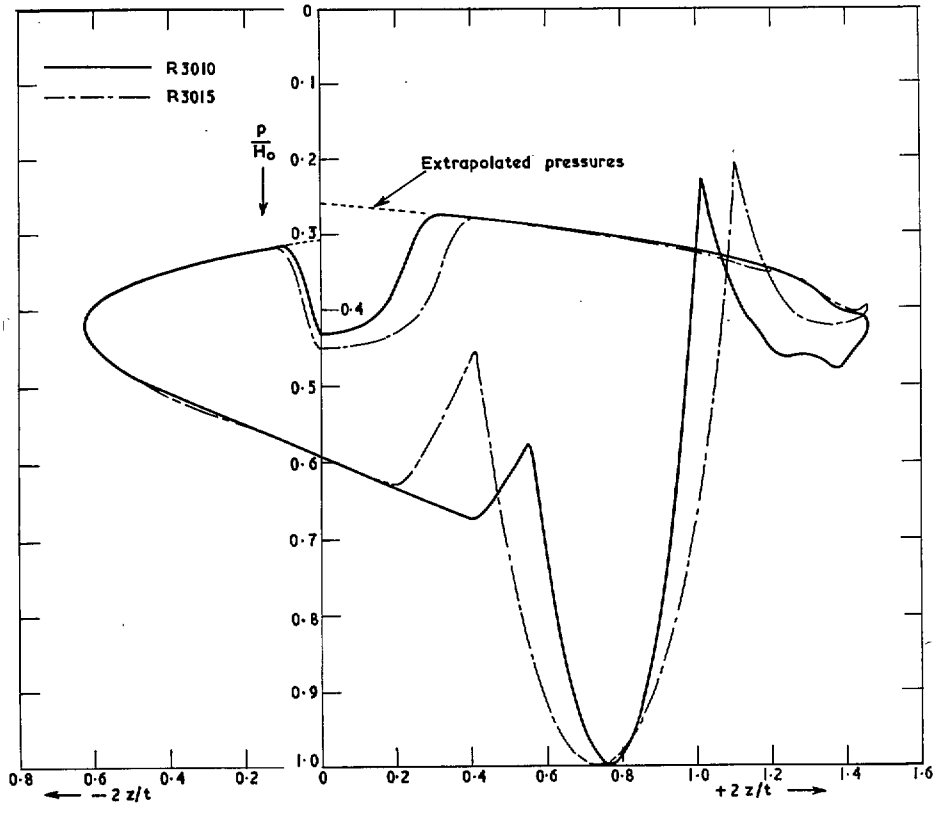

FIG. 11. Comparison of pressure distributions on sections R3010 and R3015. $M_0 = 1{\cdot}0$, $\alpha = 2^0$.

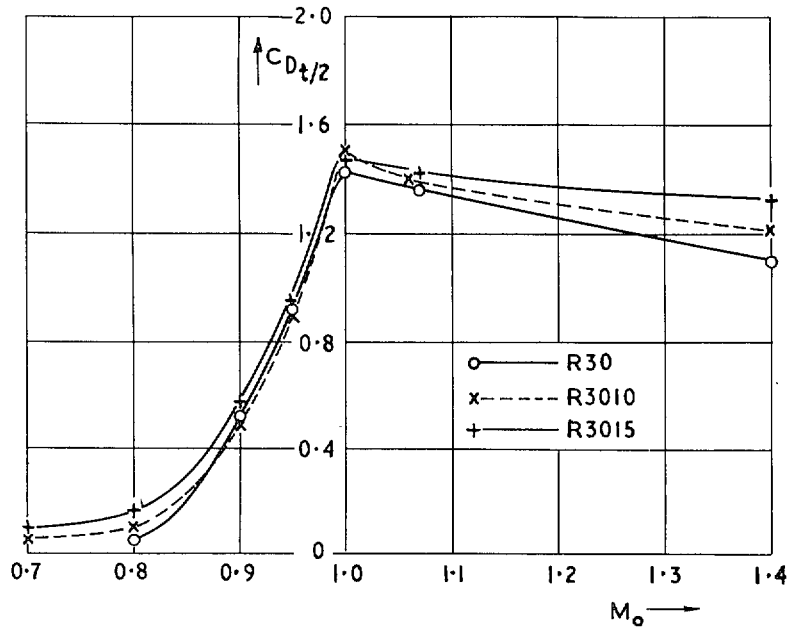

FIG. 12. Variation of measured pressure-drag coefficients with Mach number. $\alpha = 0^0$.

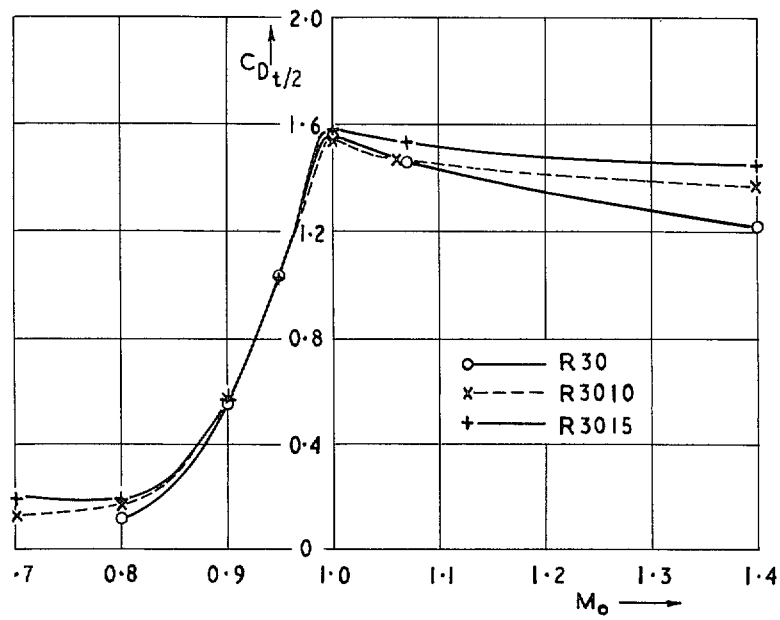

FIG. 13. Variation of measured pressure-drag coefficients with Mach number. $\alpha = 2^0$.

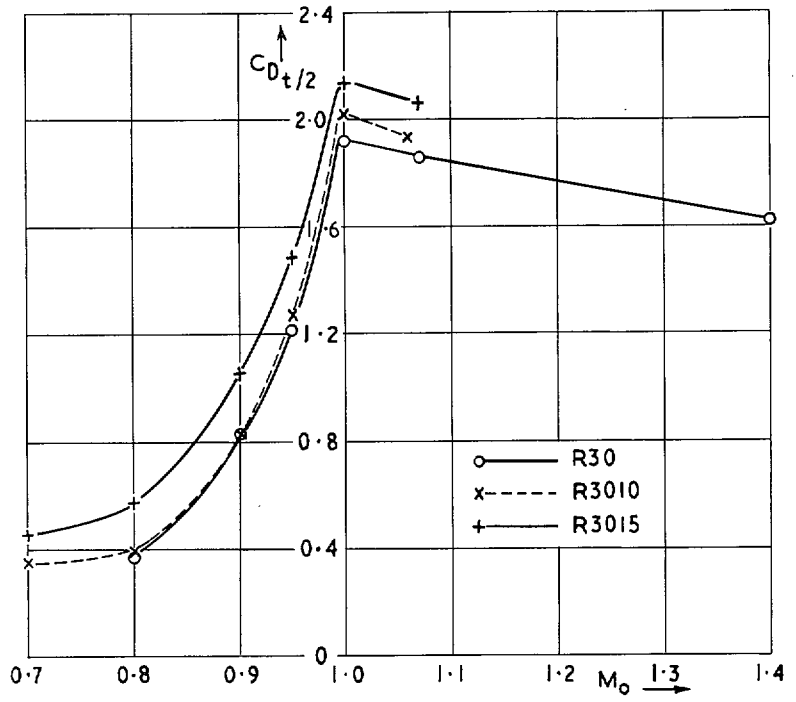

FIG. 14. Variation of measured pressure-drag coefficients with Mach number. $\alpha = 4^0$.

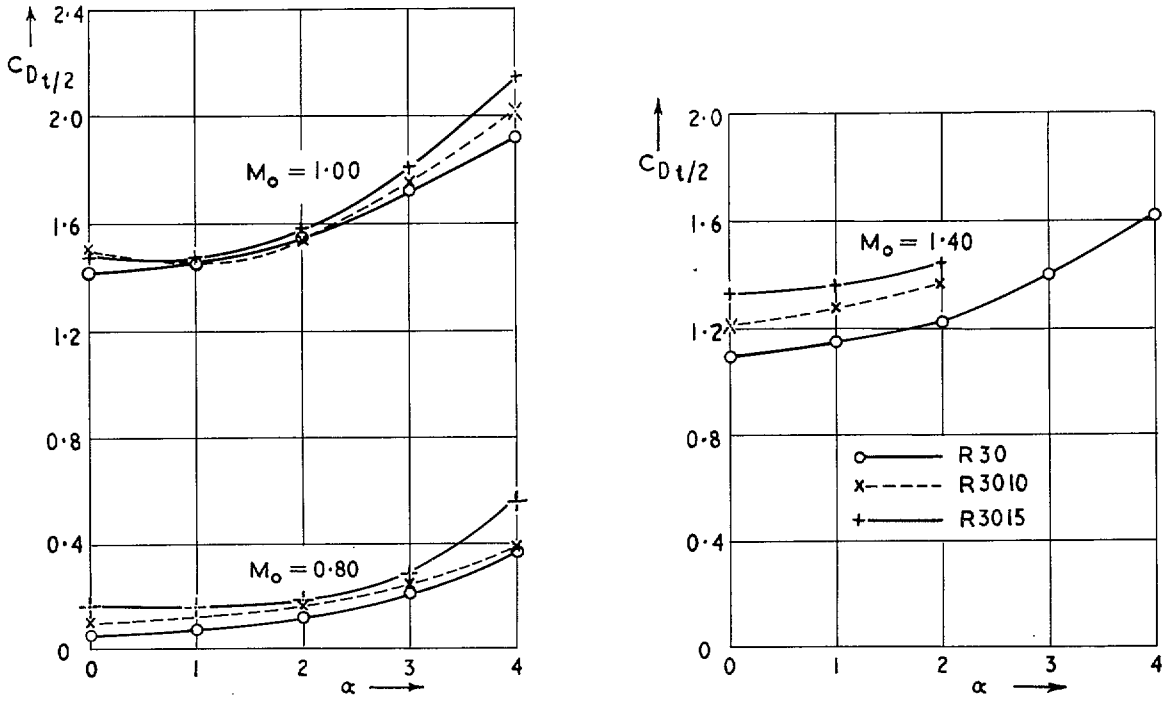

FIG. 15. Variation of measured pressure drag coefficients with incidence.

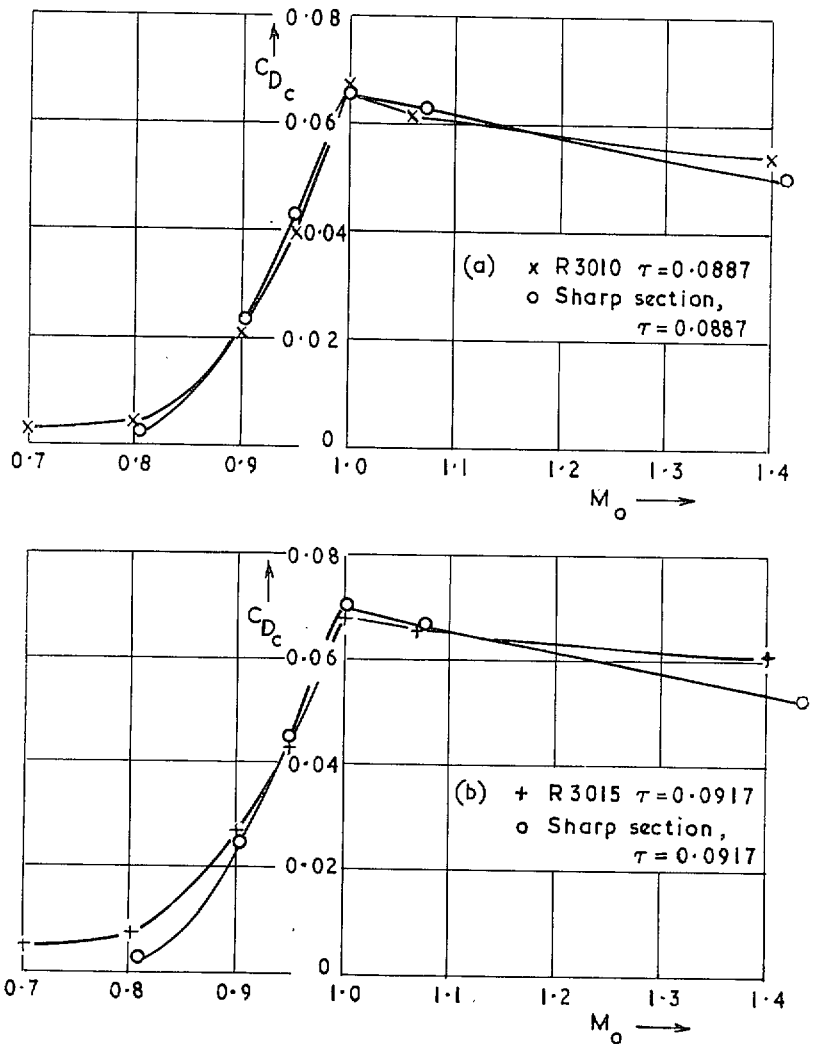

FIG. 16. Comparison of drags of R3010 and R3015 with those for sharp sections of the same thickness-chord ratio. Variation with Mach number. $\alpha = 0^0$

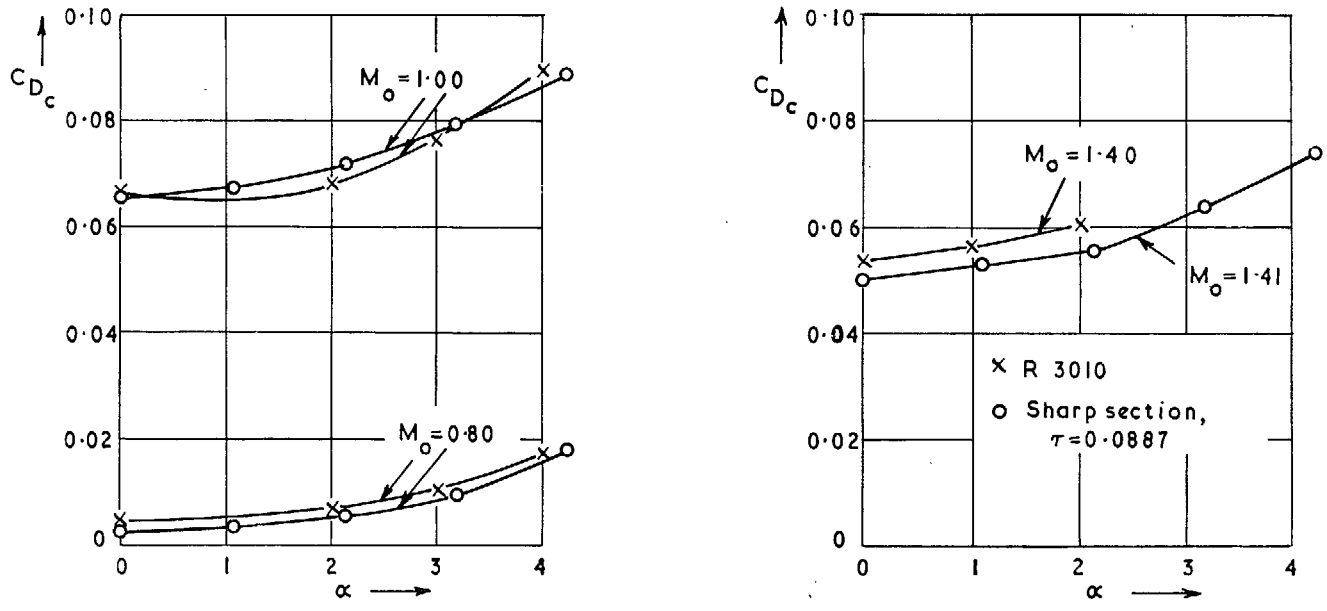

FIG. 17. Comparison of drag of R3010 with that for sharp section of same thickness-chord ratio. Variation with incidence.

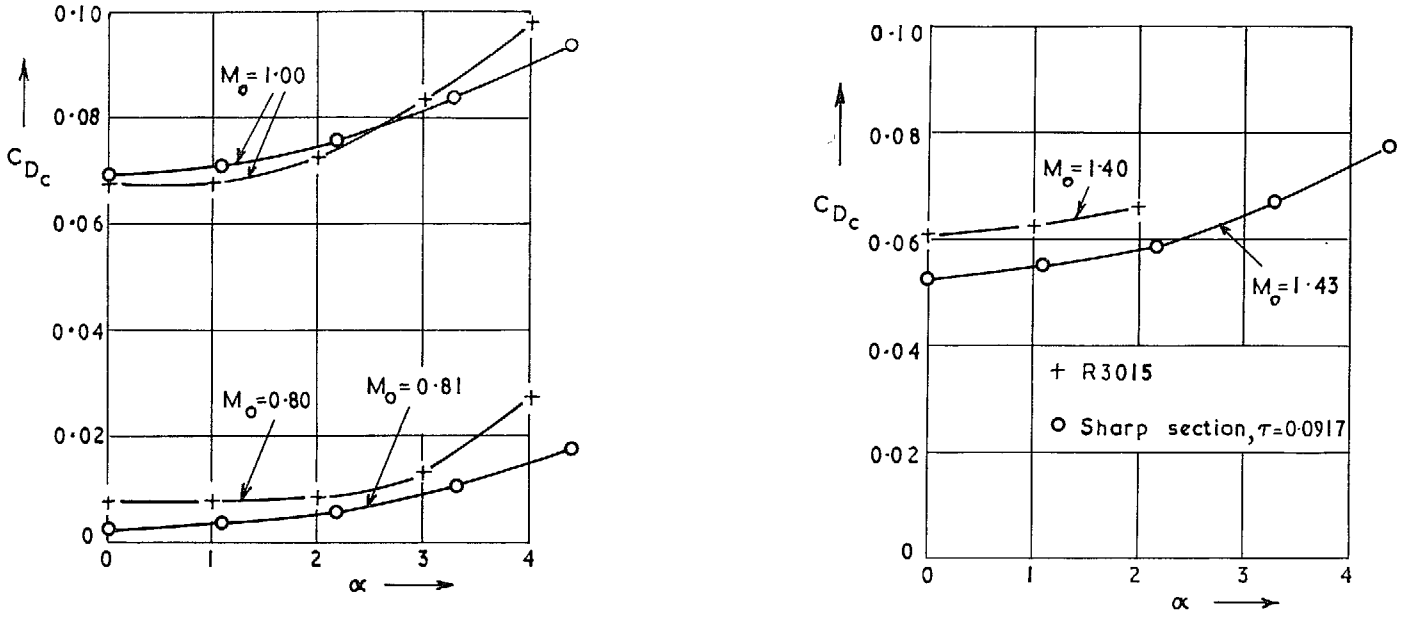

FIG. 18. Comparison of drag of R3015 with that for sharp section of same thickness-chord ratio. Variation with incidence.

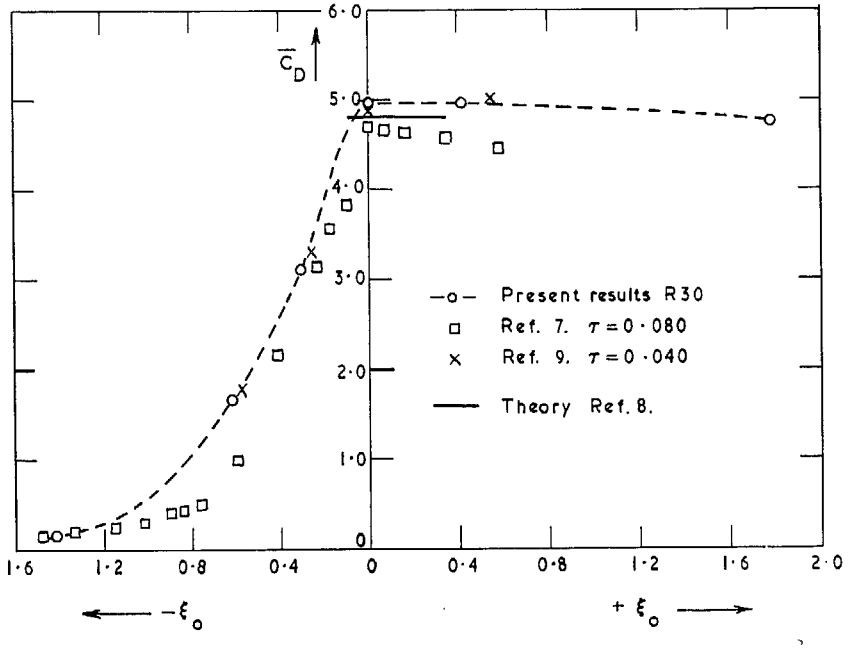

FIG. 19. Comparison of R30 drag with previous data. $\alpha = 0^0$.

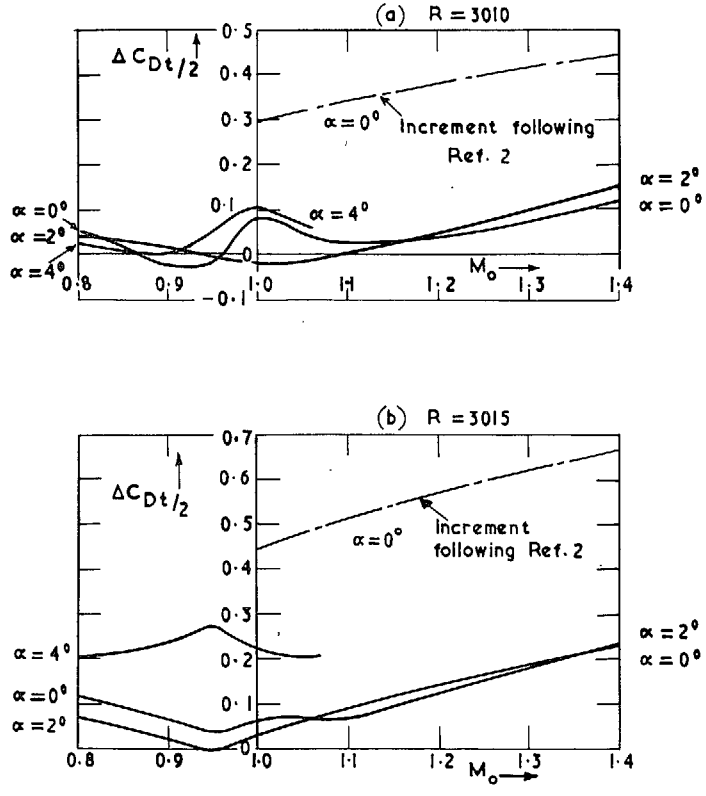

FIG. 20. Pressure-drag coefficient increment due to blunt leading edge.

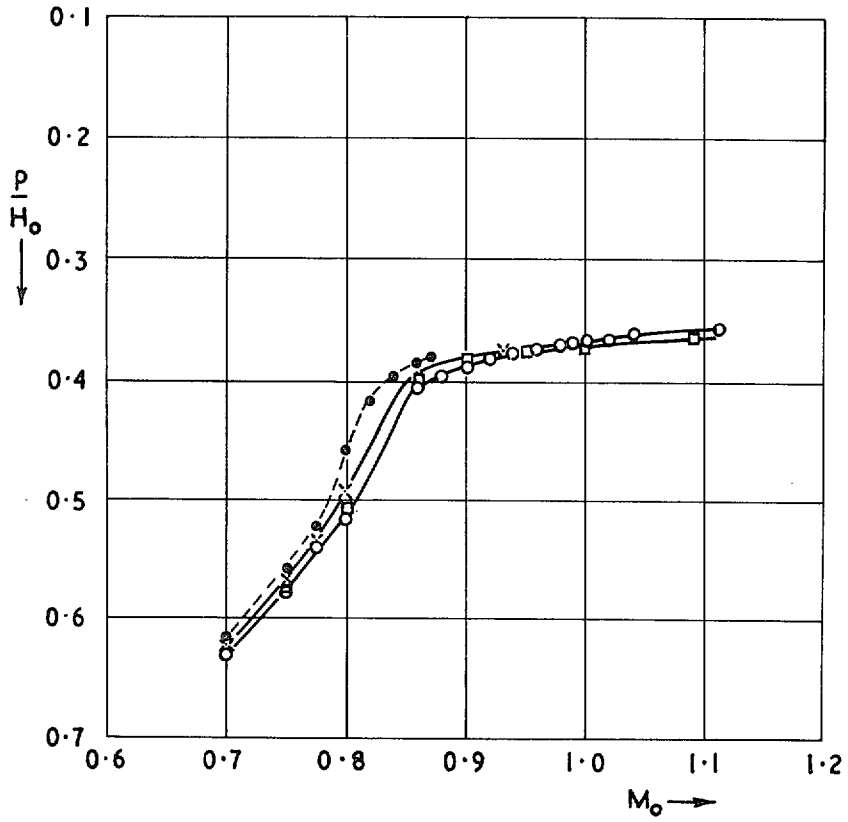

Symbol	Open area ratio (σ)	T
○	0·091	0·96
□	0·042	0·87
×	0·025	0·73
⊙	0	−1·0

FIG. 21. Variation of pressure with Mach number for different values of liner slot opening. Section RAE 104, $\alpha = 0^0$, $x/c = 0{\cdot}52$.

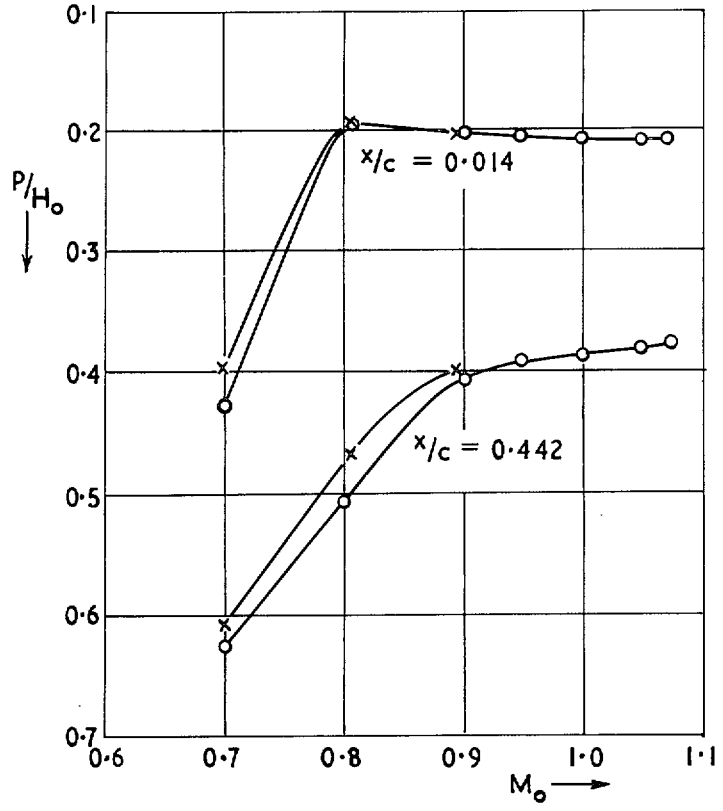

Symbol	Open area ratio (σ)	T
o	0·092	0·96
x	0·025	0·73

FIG. 22. Variation of pressure with Mach number for different values of liner slot opening. Section R3015, $\alpha = 2^{0}$.

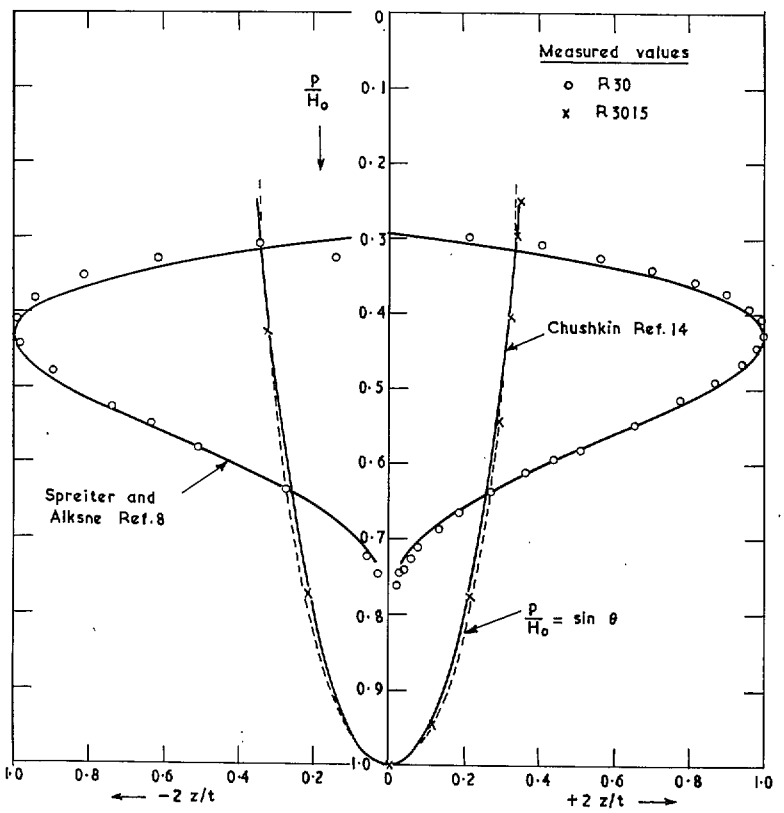

FIG. 23. Theoretical prediction of pressures on sharp section R30 and leading-edge of blunt section R3015 $M_0 = 1{\cdot}0$. $\alpha = 0$.

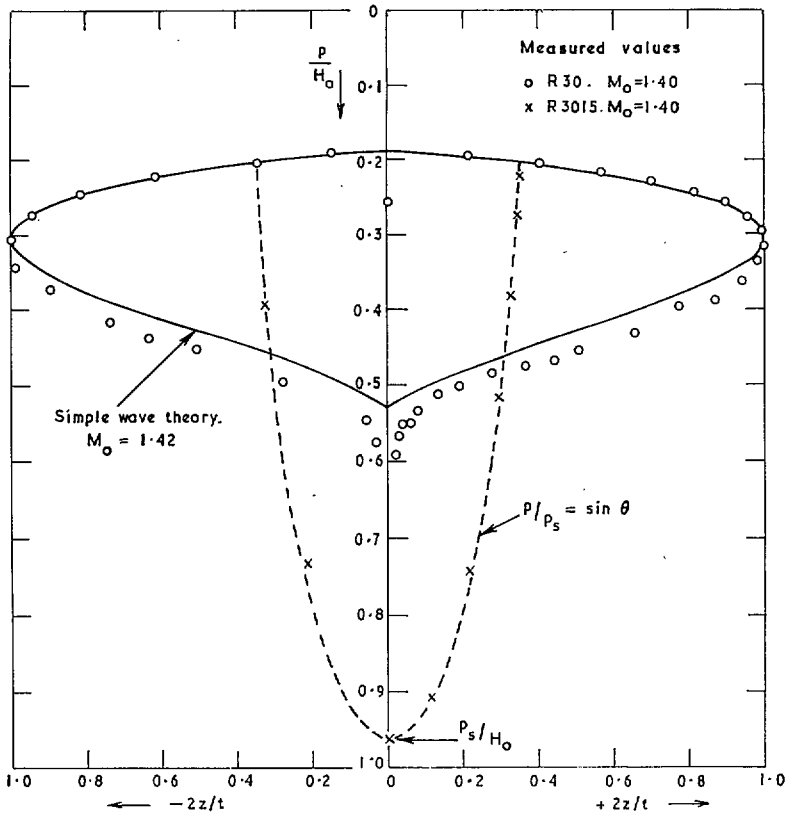

FIG. 24. Estimates of pressures on sharp section R30 and leading edge of blunt section R3015. $M_0 = 1{\cdot}40$; $\alpha = 0^0$.

Printed in Wales for Her Majesty's Stationery Office by Allens Printers (Wales) Ltd.

Dd.129527 K5 7/67 Gp.1724

Published by
HER MAJESTY'S STATIONERY OFFICE

To be purchased from
49 High Holborn, London W.C.1
423 Oxford Street, London W.1
13A Castle Street, Edinburgh 2
109 St. Mary Street, Cardiff
Brazennose Street, Manchester 2
50 Fairfax Street, Bristol 1
35 Smallbrook, Ringway, Birmingham 5
7–11 Linenhall Street, Belfast 2
or through any bookseller

S.O. Code No. 23–3465